ISSN: 0369-8963

Microwave absorbing applications: Characterization of the Electromagnetic and Mechanical Properties of Iron Reinforced Natural Fiber Composites

DR. ROBIN KUMAR SAMUEL[1,*], DR.N.KANTHAVELKUMARAN[1], DR.A.MALAR RETNA[2]

[1]Department of Mechanical Engineering, Ponjesly College of Engineering, Alamparai, Nagercoil, Tamilnadu, India – 629003

[2]Department of Chemistry and Research Centre, Scott Christian College (Autonomous), Nagercoil – 629003

[*]Correspondence to Dr.Robin Kumar Samuel

Abstract

It is still difficult to create an effective microwave absorption composite made of natural Fibers that also has strong tensile and electromagnetic properties. In this study, experiments are carried out to create new hybrid microwave absorbent composites made of jute Fibers bonded with iron. This experimental study's goal is to improve absorption and widen the absorption bandwidth while maintaining acceptable tensile properties. Hence four samples have been used been created and tested with varying iron levels and a constant jute Fiber content. The waveguide-based microwave measuring approach has been used to measure the electromagnetic parameters. It is discovered that an ideal sample has good X-band microwave absorption characteristics. Additionally, the created composite is put to the tensile test, where it is discovered to have an average Young's modulus. Current investigation to observe the values of 9.4 GPa for the modulus, 0.08 for the ultimate strain, and an average ultimate 49 MPa is the tensile strength value. Analyses using a scanning electron microscope were used for the interior failure behavior of the tensile-tested specimen and establish the primary mechanisms of failure like matrix cracking, Fiber breaking, and delamination failure. The outcomes show the potential of the manufactured composite for diverse tactical uses.

Keywords: *Composites; Electromagnetic; Jute Fiber; Microwave absorber; micro wave measurement*

Introduction

Jute has grown to be one of the most significant natural Fibers harvested from jute plants due to its low cost and high productivity. The use of jute Fibers in the production of carpets, shopping bags, and related items can be used to justify the value of jute Fibers [1]. It has good heat insulating qualities, a low weight, and high toughness [2]. Additionally, it is economical, easily accessible, completely biodegradable, and environmentally beneficial. When compared to synthetic Fibers, jute Fiber has adequate mechanical strength. Researchers have examined jute and other natural Fibers as a reinforcing agent in composites in a variety of literature works [4–6].

In the realm of low observable technology, as well as elsewhere, microwave absorbing materials and structures are actively used to reduce undesired electromagnetic interference [7]. It has been

 https://doi.org/10.37896/pd91.4/91441

ISSN: 0369-8963

investigated if various composites made of dielectric, magnetic, and conductive materials could be used as microwave absorbers [8–11]. Additionally, it has been claimed that rubber components that are embedded with carbonyl iron or other micron-sized permanent magnet fillers have good absorption properties [11–13]. Composite materials based on graphene and carbon nanotubes (CNTs) have been described as effective shielding materials. Additionally, waste composite materials are said to offer a practical, affordable answer in this direction [14].

It has been extensively documented that Meta materials, artificially engineered materials, and frequency selective surfaces (FSSs) operate as effective absorbers from radio frequencies to the terahertz frequency regime. Advanced EM filtering structures called FSSs are utilized to regulate the movement of EM waves. By combining active components, graphene, and other materials, researchers have discovered an adjustable absorption response. The majority of research on microwave absorption composites up to this point has been on using synthetic Fibers. It is difficult to create a natural Fiber-based composite that can absorb the incoming EM radiation. The microwave absorbing structures need to strike the optimum balance between their mechanical and absorption capabilities, but doing so simultaneously is challenging. There is a dearth of research on natural Fiber-based composites for microwave absorption applications. Natural Fibers are a potential option to be taken into consideration as reinforcement in the creation of an effective and affordable microwave absorbent composite given the benefits they offer and the outcomes of previous literature work. As a result, in this research, microwave absorbent composites made of iron-reinforced natural Fibers have been created and assessed between 8.2 and 12.4 GHz.

Materials and Methods

In order to create the microwave absorbent composite, iron metal powder from High Media Labs was employed as filler. The composite was reinforced with woven jute Fiber and bound with epoxy glue. Epoxy was cured with the help of the hardening agent to produce remarkable mechanical qualities. Jute Fiber, epoxy, and iron powder have relative densities of 1.5 g/cm3, 1.1 g/cm3, and 7.8 g/cm3. The ratio of the epoxy resin to the hardener was always 75:25. Following a manual mixing period of 30 minutes, an ultrasonic mixing period of 30 minutes was used to combine the iron powder with epoxy resin in specific proportions as needed for the composite. In this composition, woven jute fabric was strengthened. The 20:80 weight-to-

 https://doi.org/10.37896/pd91.4/91441

ISSN: 0369-8963

percent ratio of the Fiber matrix was maintained. According to Table 1, the iron metal powder was employed in various ratios of 35, 40, 50, and 55 percent.

Applying the mould releasing agent with a brush and allowing it to cure for 20 minutes on the acrylic board was the first step. The second stage involved placing the first layer of jute fabric on the board, and the third step involved brushing resin over this layer of jute fabric. The removal of air bubbles from the surface with the use of a roller was the fourth step. To ensure homogeneity, the roller tightly presses the jute layer against the earlier ones. Additionally, as the layers are rolled, it presses out any voids or air bubbles to lessen the possibility of trapping them. The following layers of jute fabric were positioned by repeating steps 2, 3, and 4. Samples were stored at room temperature for 48 hours after the fabrication process. The constructed sample was held in a heating furnace at a temperature of 60^{o}C for roughly 20 hours to further cure it and remove moisture. Using a waveguide-based microwave measuring system, electromagnetic characterizations of the manufactured samples were performed.

Table 1. Designation of samples with codes based on iron contents

Jute %	Matrix %		Symbol	Thickness of composite sample (mm)	Method Utilized
	Iron	Epoxy			
20	35	45	A	4.1	Hand layup
20	40	40	B	5.9	Hand layup
20	50	30	C	6.5	Hand layup
20	55	25	D	6	Hand layup

At X-band, the frequency-dependent dielectric and magnetic characteristics of the samples were investigated (i.e. 8.3 to 12.5 GHz). The measuring set-up consists of a waveguide calibration kit, a sample holder, and a handheld vector network analyzer [15]. One of the biggest risks in microwave measurements is the presence of an air gap between the waveguide and the sample holder, which is why the rectangular samples have been put inside the sample holder. The tests have been performed using the WR90 waveguide, a US standard. As a result, using the scattering parameters, electromagnetic parameters in terms of complex dielectric permittivity and complex magnetic permeability values have been determined (transmission and reflection coefficients). At room temperature, all measurements were taken.

 https://doi.org/10.37896/pd91.4/91441

ISSN: 0369-8963

A hand layup technique was used to create a composite plate with dimensions of 200 mm, 100 mm, and 7.5 mm in order to assess the tensile reaction. Jute, iron, and epoxy made up 20, 40, and 50% of the composite's weight, respectively. According to the provided formula [3],

$$V_i = \frac{m_i/\rho_i}{m_{jute}/\rho_{jute} + m_{iron}/\rho_{iron} + m_{epoxy}/\rho_{epoxy}}$$

The figures reported in accordance with the aforementioned relation were 28, 59, and 13%, respectively. Weaved jute cloth was strengthened in this combination after 20–30 minutes of manual mixing of iron and epoxy and 30 minutes of ultrasonic stirring. After manufacturing, samples were given 48 hours to progressively cool at room temperature.

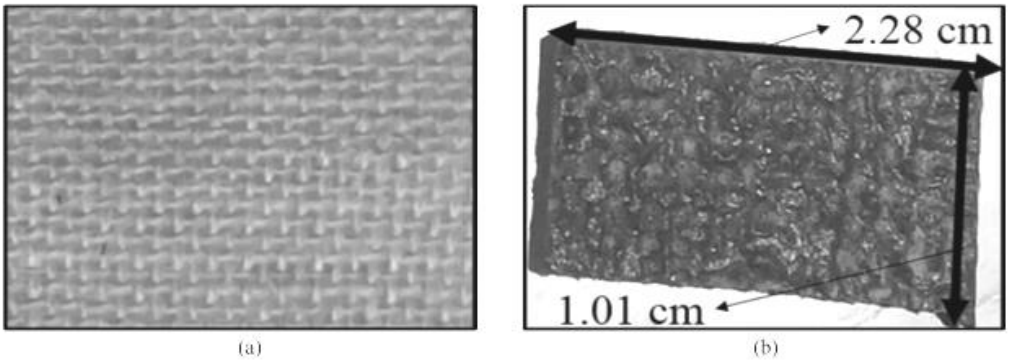

Figure 1. (a) Jute fabric used to prepare the specimen for electromagnetic testing, (b) Electromagnetic testing

The manufactured sample was heated to 60ºC for approximately 20 hours in order to further cure it. The sample was then divided into two identically accurate tensile test specimens with forms in accordance with GOST 25.601 using water jet machining. The volume percentages of jute, iron, and epoxy were hypothetically determined standard. At the Defense Research and Development Laboratory (DRDL), Hyderabad, India, cured specimens were put through tension tests utilizing a universal testing apparatus as illustrated in Fig. 1. (c).

https://doi.org/10.37896/pd91.4/91441

ISSN: 0369-8963

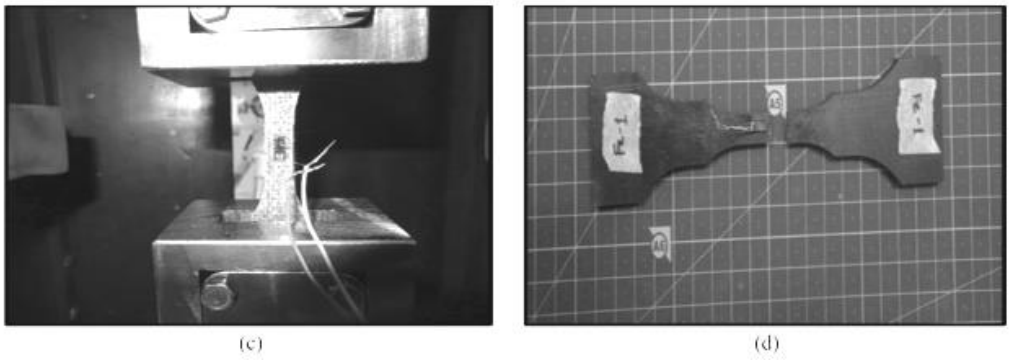

Figure 1. (c) tensile test specimen and (d) failure under tension.

The gauge length was calculated to be 20 mm, while the narrow section's width was 10 mm. It was established that the specimen's thickness was 7.5 mm, and that the narrow section's size was 75 mm^2. To determine Young's modulus, the tensile test was conducted on two samples, and the ultimate tensile strength and average of the data from the tests conducted on both samples were taken. At first, samples were examined up to the proportionate limit, and two separate set readings were recorded. Each set of values from the tests were used to create stress-strain curves. The Young's modulus values for each set of data are given by the slope of these curves. These values' averages were assessed. Then, a tensile force was applied to two specimens until failure occurred.

Result and Discussion

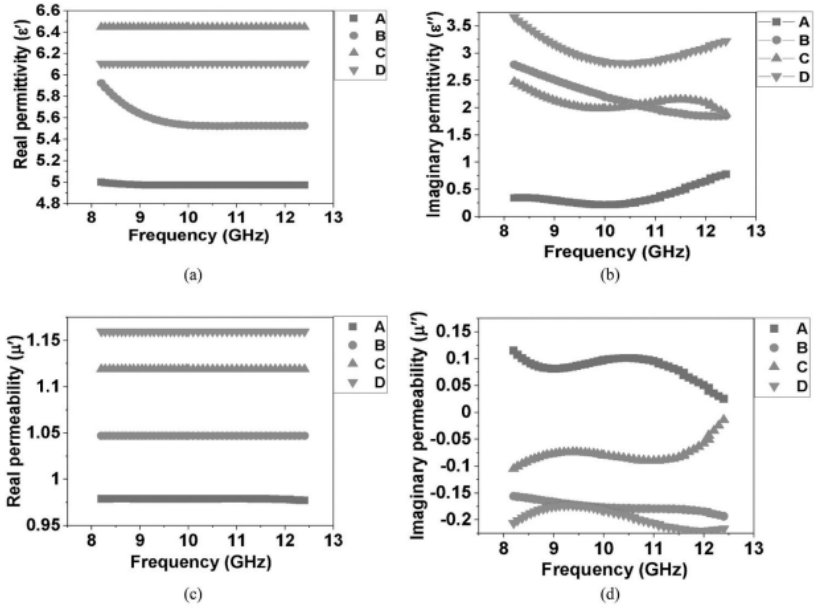

Figure 2. Variation of EM parameters with frequency (a) Real permittivity, (b) Imaginary permittivity, (c) Real permeability, (d) Imaginary permeability.

 https://doi.org/10.37896/pd91.4/91441

ISSN: 0369-8963

Figures 2 show the frequency-dependent ε', ε", μ', and μ" values of artificial samples (a-d). For samples A, C, and D, the polarization of electric dipoles oscillates in phase with the electric field vector, which is what causes 0 to be independent of frequency as seen in Figure 2. (a). Contrary to this pattern, in sample B, dipoles do not respond to changes in the electric field until frequency exceeds 10 GHz. This is the cause of the decrease in the value of ε' up to 10 GHz and the subsequent almost constant value of 5.5. The samples C and A yielded the highest and lowest reported values of 0, 6.44 and 4.99, respectively. The fluctuation of ε'' with frequency for each of the samples, A, B, C, and D, is shown in Fig. 2(b). Sample D initially exhibits a drop in ε'' value down to 2.82. Following this, it has been seen that the value of ε'' rises, reaching a maximum value of 3.22. Sample C displays a persistent decreasing and growing trend in the value of ε'', initially dropping down to 1.984 before increasing and then beginning to decrease once more at 2.152. The value of ε'' in Sample B continuously decreases from 2.79 to 1.84. Sample A displays reduced fluctuation from ε'' to 0.215, which eventually rises to 0.78. The highest value of ε00, which was observed for sample D, is 3.66. Samples A, B, C, and D's average values of ε00 are 0.3701, 2.2, 2.104, and 3.04, respectively.

The relationship between μ' and frequency is depicted in Figure 2(c). For all samples, the variance of μ' in terms of frequency is still quite small. This is caused by magnetic dipole polarization being in phase with the magnetic field vector. For samples A and D, the highest and minimum values of μ' are 1.159 and 0.98, respectively. As can be observed, the value of μ' increases along with the sample's iron concentration. Magnetic loss tangent fluctuation between 8.2 and 12.4 GHz is depicted in Figure 3(b). The graph demonstrates that each sample exhibits curves with continuously growing and declining tendencies. It can be shown that the maximum values of the dielectric loss and magnetic loss tangents obtained are 0.6 for sample D and 0.11 for sample A, respectively, demonstrating that dielectric losses prevail over magnetic losses in the constructed composite specimens and play a substantial role in supplying absorption qualities.

Figures 3(c) and 3(d), respectively, show the values for skin depth and frequency-dependent microwave conductivity. Figure 3(c) shows that the conductivity's fluctuation with frequency is not particularly strong. This might be because the electric field and the vibrations of the filler particles are in phase. Due to the presence of a lot of filler, Sample D had the greatest conductivity of all the samples at 2.22 S/m. Conduction occurs through the tunneling process at low filler contents because there are not enough filler particles to build conductive networks.

 https://doi.org/10.37896/pd91.4/91441

ISSN: 0369-8963

Currents created through this method are referred to as tunneling currents. Sample D had the highest average microwave conductivity, measuring 1.736 S/m.

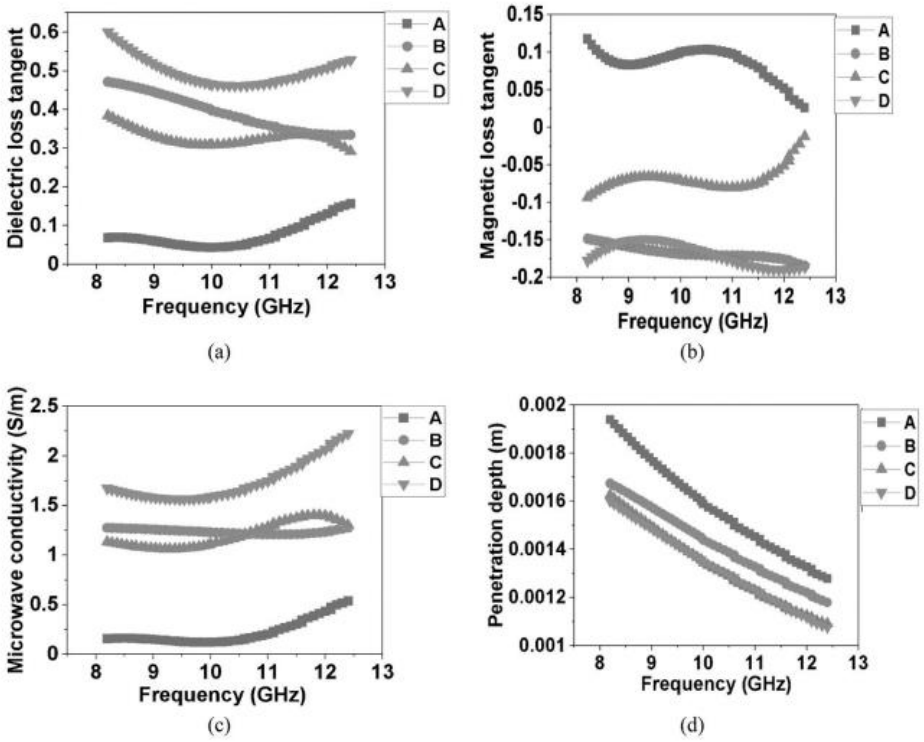

Figure 3. Variation with frequency (a) Dielectric loss tangent, (b) Magnetic loss tangent, (c) Microwave conductivity, and (d) Penetration depth.

Figure 3 shows how skin depth varies as a function of frequency (d). Smaller penetration depth values indicate that polarization occurs quickly due to higher conduction. Additionally, a linear relationship between penetration depth and conductivity can be stated to exist. Due to its low filler content, Sample A exhibits the maximum penetration depth of 1.94 mm since the incident EM wave does not easily attenuate after getting incident on the material. Due to their large filler contents, Samples C and D have low values for skin depth. The deeper the penetration, the more EM energy is lost due to higher conductivity, which also causes EM waves to attenuate more quickly inside the material. Sample D had the lowest penetration average (1.32 mm).

https://doi.org/10.37896/pd91.4/91441

ISSN: 0369-8963

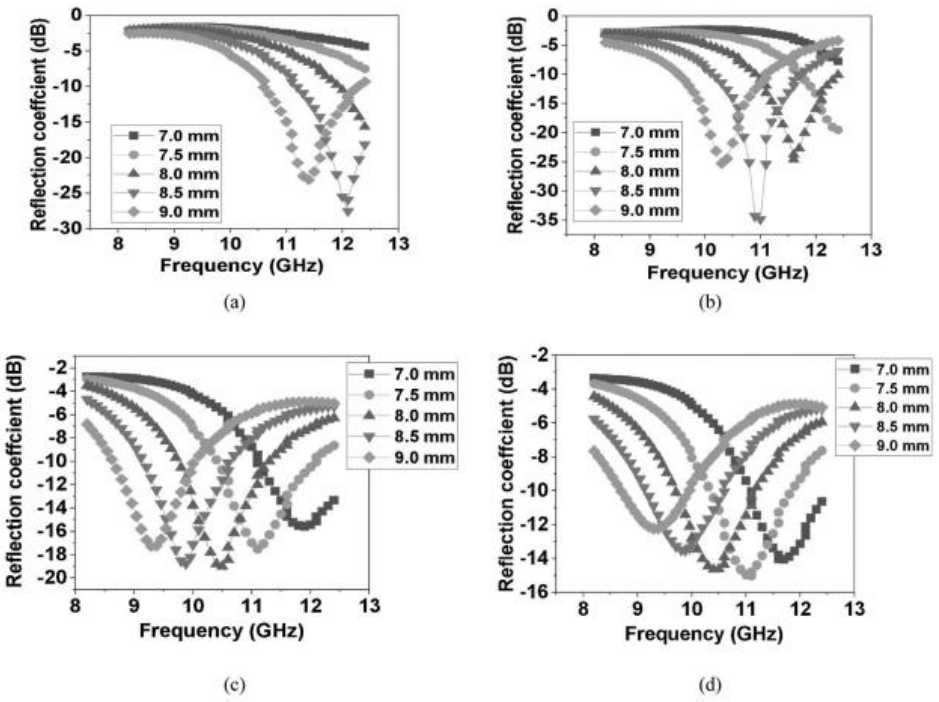

Figure 4. Variation of reflection coefficient with frequency at different thickness values for (a) sample A, (b) sample B, (c) sample C, and (d) sample D.

Figures 4(a) through (d) depict the frequency-dependent change of reflection coefficients (RC) for various thickness levels. The absorber layer thicknesses of 8.0, 8.5, and 9.0 mm are the only ones that yield the absorption bandwidth (ABW) for sample A. At 8.5 mm in thickness, sample A's minimum value of RC is 27.5 dB. Furthermore, at a thickness of 9.0 mm, this sample's greatest bandwidth was 1.5 GHz. At 8.5 mm in thickness, sample B's minimum value of RC is 34.8 dB. In addition, the highest known bandwidth is 1.6 GHz at a 9.0 mm thickness. One can see that with sample B's 7.0 mm thickness, no ABW was obtained.

The sample C at 7.5 mm thickness measured an ABW of 1.7 GHz, which is the highest value recorded. Figures 4(a-d) demonstrate that for a specific sample, the minimum value of RC reduces up to a certain thickness value before beginning to increase as the thickness is increased further. Additionally, when thickness increases, the RC curve moves to lower frequency areas. The average absorption percent values for samples A through D are 88.3, 96.2, 98.1, and 95.7, respectively. The sample C average absorption is the greatest at 98.1%.

The dielectric loss tangent of Sample D is the highest, whereas the magnetic loss tangent is the lowest. Additionally, the magnetic loss tangent in sample B is more considerable. Compared to magnetic losses, the impact of dielectric losses on the absorption properties is more

 https://doi.org/10.37896/pd91.4/91441

ISSN: 0369-8963

significant. Due to the combined effects of magnetic and dielectric losses, sample B's RC value is at its lowest, which is understandable. The sample C ABW is the highest. This might be as a result of its strong polarization properties over a wider frequency range, which is explained by its high dielectric constant values. The sample C thickness of 7.5 mm yields the maximum value of ABW, one may infer. RC for Sample B is 34.8 dB for an 8.5 mm thickness measurement made at 11 GHz. For sample D at 11.1 GHz, the reflection coefficient has a minimum value of 15 dB. When compared to other samples, Sample D has an RC of 19 dB at the thinnest value, yet it still cannot be used for RAC because the ABW it offers is the lowest of the four samples. Despite having large thickness values, Samples A and B exhibit good absorption capabilities. One may conclude that the maximum value of ABW is produced by the sample C thickness of 7.5 mm. For an 8.5 mm thickness measurement taken at 11 GHz, the RC for Sample B is 34.8 dB. The reflection coefficient has a minimum value of 15 dB for sample D at 11.1 GHz. Sample D has an RC of 19 dB at the thinnest value when compared to the other samples, yet it still cannot be used for RAC because it delivers the lowest ABW of the four samples. Although Samples A and B have high thickness values, they have good absorption properties. The composite in the current study has the same mechanical properties in both longitudinal and transverse directions thanks to the usage of woven jute cloth (directions 1 and 2).

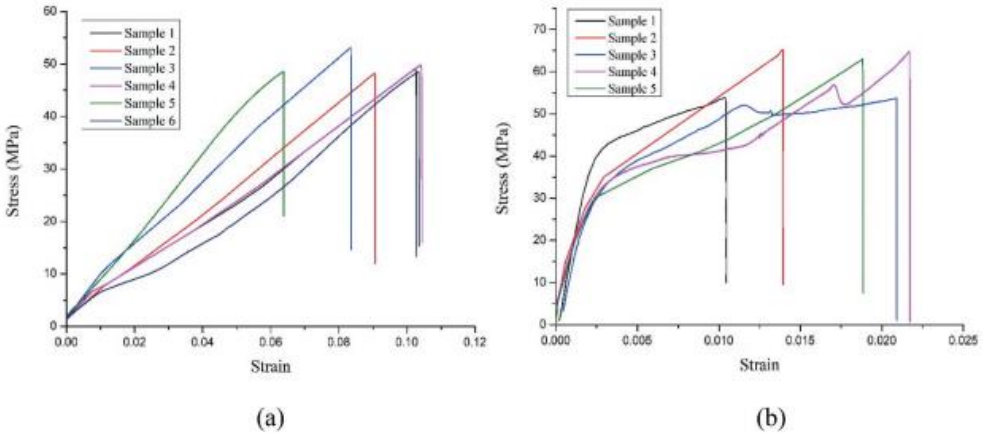

Figure 5. Stress-Strain curves of (a) Jute-Fe composite samples (b) Jute composite samples.

The prepared composite has been presumptively assumed to be transversely isotropic, and as a result, properties such as longitudinal ultimate tensile strength, longitudinal Young's modulus, and longitudinal yield strength in direction 1 (U11,E11,Y11) have been considered equal to the transverse ultimate tensile strength, transverse Young's modulus, and transverse yield strength in direction 2 (U22,E22,Y22), i.e. Y11 14. According to reports, the sample's

 https://doi.org/10.37896/pd91.4/91441

ISSN: 0369-8963

average values for ultimate tensile strength (U11), tensile modulus (E11), and yield strength (Y11) are approximately 49 MPa, 9.4 GPa, and 3.92 MPa, respectively.

There was a reduction in tensile strength when compared to samples without iron. Tensile stress-strain curves for both composites are shown in Figures 5(a) and 5(b) up until specimen failure. The composite can withstand a maximum load of about 3681 N on average. The composite specimen fails at an average stress of about 49 MPa, and the associated average strain is 0.08. In contrast to Figure 5(a), the stress-strain curve had a slight nonlinearity 5(b).

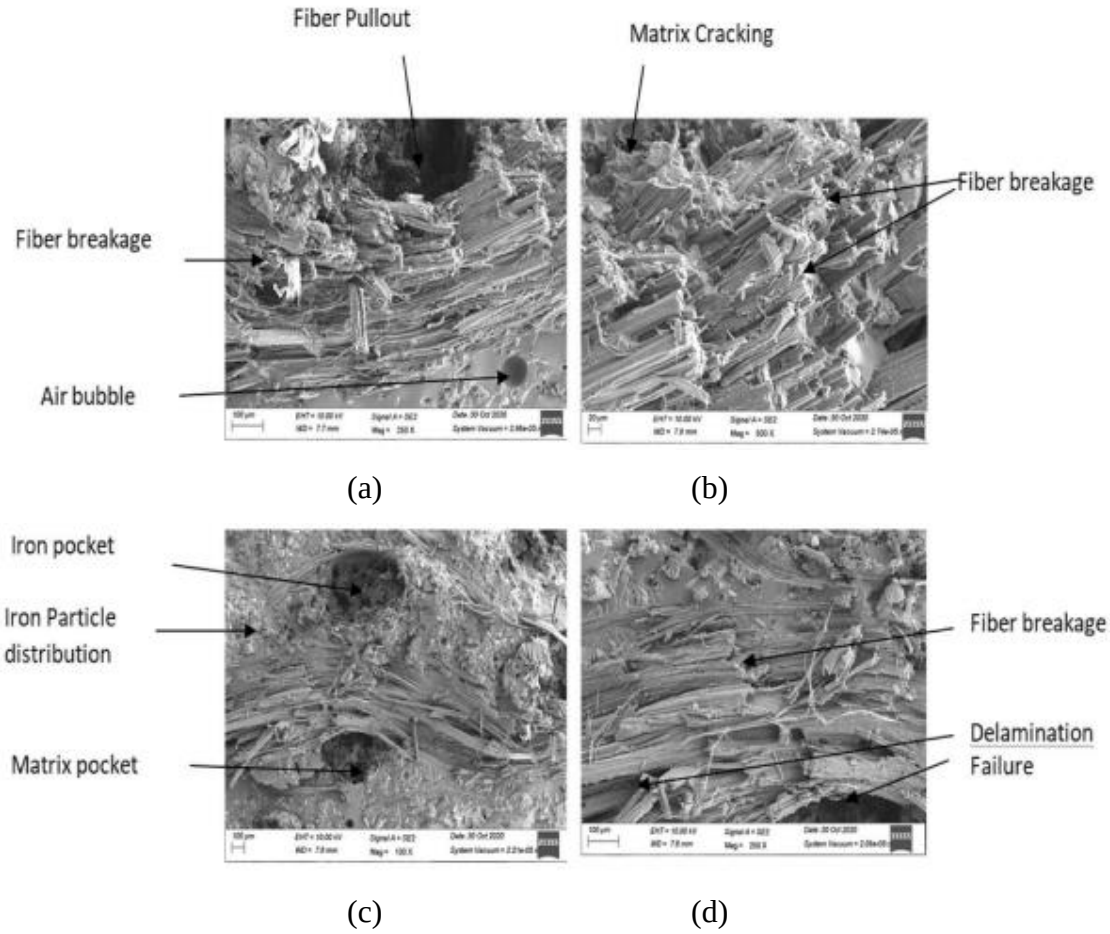

Figure 6. SEM images - Different modes of failure for the fabricated jute fiber composites (a) Fiber breakage and pullout, (b) Matrix cracking and fiber breakage, (c) Iron pocket, resin pocket, and iron particle distribution (d) Delamination failure and fiber breakage.

Its behavior could be attributed to the composite's lower Fiber volume fraction (28 percent for the Jute-Fe composite sample versus 38 percent for the Jute composite sample), higher brittleness from the addition of iron as a filler, and various failure mechanisms (including Fiber, matrix, and debonding) [2]. To create accurate computational modeling for a variety of

 https://doi.org/10.37896/pd91.4/91441

ISSN: 0369-8963

structural applications, all the EM characteristics and mechanical properties discussed above must be taken into consideration. Figure 6 (a-b-c-d) displays SEM images of samples and illustrates the interior failure behavior of the jute Fiber composite for tensile tests. The image made evident that there was matrix fracture, Fiber pullout, resin pockets, debonding, and delamination failure. The Fibers' final breakdown or withdraw, which occurred without any discernible elongation, mimicked the brittleness of jute Fiber.

Stress was concentrated because of the existence of resin pockets close to the interlacing, which reduced the ability of the Fiber and matrix to transfer loads. During the tensile tested specimen, inter- and intra-laminar delamination failure was also seen between the plies and with the ply.

Conclusions

The creation of iron-reinforced natural Fiber-based composites with encouraging microwave absorption capabilities was accomplished in this study using a unique method. The depth of penetration, reflection coefficient, and frequency-dependent EM characteristics provide strong support for the findings. The sample for tensile testing to ascertain Young's modulus and ultimate tensile strength was constructed using the optimal iron weight ratio and thickness value. To forecast the Fiber failure, inter laminar failure, and intra-laminar delamination failure behavior for the Jute Fiber composite, SEM analysis was carried out on the tensile tested specimen. An important study was conducted to characterize the electromagnetic characteristics and the mechanical properties for a number of structural applications using effective design and creation of realistic computer modeling.

References

1. ALAM M M., MANIRUZZAMAN M., MORSHED M M.: Application and advances in micro processing of natural Fiber (jute)–based composites, *Compr Mater Process*., **7**, 243–260, (2014)
2. PATEL S., AHMAD S.: Probabilistic failure of Graphite Epoxy Composite plates due to low velocity Impact, *ASME*., **139 (4),** 044501-4, (2017)
3. DALBEHERA S., ACHARYA S K.: Study on mechanical properties of natural fiber reinforced woven jute-glass hybrid epoxy composites, *Adv Polym Sci Technol.*, **4 (1)**, 1–6, (2014)

 https://doi.org/10.37896/pd91.4/91441

ISSN: 0369-8963

4. TINGJU LU., SHIMENG LIU., MAN JIANG., XIAOLING XU., YONG WANG., ZEYONG WANG., JAN GOU., DAVID HUI., ZUOWAN ZHOU.: Effects of modifications of bamboo cellulose fibers on the improved mechanical properties of cellulose reinforced poly(lactic acid) composites, *Compos Part B.*, **62**, 191–197, (2014)
5. GUJJALA RAGHAVENDRA., SHAKUNTALA OJHA., ACHARYA S K., PAL S K.: Jute fiber reinforced epoxy composites and comparison with the glass and neat epoxy composites, *J Compos Mater.*, **48 (20)**, 2537– 2547, (2014)
6. WECLAWSKI B T., FAN M., HUI D.: Compressive behavior of natural Fiber composite, *Compos Part B.*, **67**,183–191, (2014)
7. PANWAR R., SON D., LEE J R.: Novel optimization method of single square FSS impinged and cascaded radar-absorbing composites, *Adv Compos Mater.*, **27**, 1–11, (2018)
8. PANWAR R., LEE J R.: Progress in frequency selective surface-based smart electromagnetic structures: a critical review, *Aerosp Sci Technol.*, **66**, 216–234, (2017)
9. PANWAR R., PUTHUCHERI S., SINGH D.: Experimental demonstration of novel hybrid microwave absorbing coatings using particle-size-controlled hard–soft ferrite, *IEEE Trans Magn.*, **54 (11)**, 1–5, (2018)
10. Micheli D., Apollo C., Pastore R., Marchetti M.: X-Band microwave characterization of carbon-based nano composite material, absorption capability comparison and RAS design simulation, *Compos Sci Technol.*, **70(2)**, 400–409, (2010)
11. ZHIGUANG DING., SHELDON Q. SHI., HUALIANG ZHANG., LIPING CAI.: Electromagnetic shielding properties of iron oxide impregnated kenaf bast fiberboard, *Compos Part B.*, **78**, 266–271, (2015)
12. BANDARU A K., PATEL S., SACHAN Y., AHMAD S, ALAGIRUSAMY R., BHATNAGAR N.: Mechanical behaviour of 3Dangle-interlock Kevlar/basalt reinforced polypropylene composites. *Polym Test*., **55**, 238 – 46, (2016)
13. CHANGLEI XIA., JASON YU., SHELDON Q SHI., YING QIU., LIPING CAI., FELIXWU H., HAN REN., XU NIE., HUALIANG ZHANG.: Natural fiber and aluminum sheet hybrid composites for high electromagnetic interference shielding performance, *Compos Part B.*, **114**, 121–127, (2017)
14. YADAV R., PANWAR R., SINGH D.: Extended Jaya's Algorithm for optimal design of broadband layered microwave absorbing structures, *IEEE Magn Lett.*, **9** , 1–5, (2018)
15. PANWAR R., LEE J R.: Performance and non-destructive evaluation methods of airborne radome and stealth structures, *Meas Sci Technol.*, **29(6)**, 062001, (29pp), (2018)

 https://doi.org/10.37896/pd91.4/91441